

Supplement of

Offline analysis of the chemical composition and hygroscopicity of sub-micrometer aerosols at an Asian outflow receptor site and comparison with online measurements

Yange Deng^{1,2,3}, Hiroaki Fujinari¹, Hikari Yai¹, Kojiro Shimada^{4,5}, Yuzo Miyazaki⁶, Eri Tachibana⁶, Dhananjay K. Deshmukh⁷, Kimitaka Kawamura⁷, Tomoki Nakayama^{2,8}, Shiori Tatsuta⁴, Mingfu Cai^{9,10}, Hanbing Xu⁹, Fei Li^{11,12}, Haobo Tan¹¹, Sho Ohata^{13,14,15}, Yutaka Kondo¹⁶, Akinori Takami¹⁷, Shiro Hatakeyama^{4,18}, and Michihiro Mochida^{1,2}

¹ Graduate School of Environmental Studies, Nagoya University, Nagoya, 464-8601, Japan

² Institute for Space-Earth Environmental Research, Nagoya University, Nagoya, 464-8601, Japan

³ Now at National Institute for Environmental Studies, Tsukuba, 305-8506, Japan

⁴ Faculty of Agriculture, Tokyo University of Agriculture and Technology, Tokyo, 183-8538, Japan

⁵ Now at Department of Chemistry, Biology, and Marine Science, University of the Ryukyus, Okinawa, 903-0213, Japan

⁶ Institute of Low Temperature Science, Hokkaido University, Sapporo, 060-0819, Japan

⁷ Chubu Institute for Advanced Studies, Chubu University, Kasugai, Aichi, 487-8501, Japan

⁸ Now at Graduate School of Fisheries and Environmental Sciences, Nagasaki University, Nagasaki, 852-8521, Japan

⁹ School of Atmospheric Sciences, Sun Yat-sen University, Zhuhai, Guangdong, 519082, China

¹⁰ Now at Institute for Environmental and Climate Research, Jinan University, Guangzhou, Guangdong, 511443, China

¹¹ Institute of Tropical and Marine Meteorology, China Meteorological Administration, Guangzhou, 510-640, China

¹² Now at Xiamen Key Laboratory of Straits Meteorology, Xiamen Meteorological Bureau, Xiamen, 361012, China

¹³ Department of Earth and Planetary Science, The University of Tokyo, Tokyo, 113-8654, Japan

¹⁴ Now at Institute for Space-Earth Environmental Research, Nagoya University, Nagoya, 464-8601, Japan

¹⁵ Now at Institute for Advanced Research, Nagoya University, Nagoya, 464-8601, Japan

¹⁶ National Institute of Polar Research, Tokyo, 190-8518, Japan

¹⁷ National Institute for Environmental Studies, Tsukuba, 305-8506, Japan

¹⁸ Now at Asia Center for Air Pollution, Japan Environmental Sanitation Center, Niigata, 950-2144, Japan

Correspondence to: Michihiro Mochida (mochida@isee.nagoya-u.ac.jp)

Text S1: Data screening and handling of filter samples

The RH and temperature values were recorded every 5 s during offline experiments using HTDMA. For derivation of the hygroscopic growth factors, only data obtained when the RH values at the outlet of DMA2 during a voltage scan (3 min) were used when they fulfilled the following two criteria: 1) the absolute difference between the mean and setting RH values was less than 0.5 %; 2) the absolute standard deviation of the RH values was less than 0.2 %.

Chemical analyses of OC/EC, WSOC, and ions were performed two or more times for a series of samples. Results from the last series of the analyses for all samples were regarded as the most reliable and were used for this study. As described in our earlier report, sampling of PM_{0.95} on 8 × 10 inch filters accompanies high loading of aerosol samples at the corners and edges of the effective sampling area (Chen et al., 2017). At least for the last series of quantification using ion chromatograph, carbon analyzer, and TOC analyzer (for WSOC), we specifically devoted attention to avoiding the use of aerosol samples at the corners and edges of the effective sampling area. Positions of the effective sampling area were assumed to be at the center of the filters, although they must have differed slightly from sample to sample. The available record of the positions for TOC analysis is incomplete but there is no indication of the use of punches at edges/corners. Although this non-uniformity was not considered at the time of sample extraction for HTDMA and offline-AMS analyses, good agreement between the calculated atmospheric concentrations of WSOM from the TOC analysis and the OM:OC of WSOM and those from the AMS analysis alone (Text S5, Fig. S5) indicates that bias from non-uniformity, even if it exists, is expected to be slight.

Malfunction of the chopper in the AMS occurred during its online W-mode operation in Okinawa in the period of 28–31 October 2015. The period from the first to the last cases that airbeam correction factor was greater than 1.2 was estimated to be under the influence of the malfunction. The W-mode data during the period were excluded from the analysis.

Text S2: Calibration of DMA size selection

Size selection of the two DMAs in the HTDMA for offline analysis was assessed by measuring the number–size distributions of 55, 100, 309, and 498 nm standard size PSL particles (models SC-0055-D, SC-0100-D, and SC-032-S, JSR, and model 3500A, Thermo Fisher Scientific Inc.) followed by determination of their mode diameters by fitting. Whereas the measured mode diameters of 100 and 309 nm PSL particles were within the prescribed expanded uncertainty ranges, the measured mode diameters of 55 and 498 nm PSL particles were greater than the upper ends of the manufacturers' warranties: 10.4 % and 1.91 %, respectively, for 55 and 498 nm particles (Table S2). Differences for

55 and 498 nm are not expected to influence the analyses greatly because the set diameter of DMA1 was 100 nm and because the measured hygroscopic growth factors of the WSM samples were within the range of 0.98–1.88, corresponding to diameters of 98–188 nm. The size selection of SMPS for the online atmospheric measurement was also assessed by measuring the number–size distributions of 55, 100, 309, and 498 nm standard size PSL particles (models are given above). Whereas the measured mode diameters of 55 nm PSL particles were 9.6 % greater than the upper end of the manufacturer’s warranty, the measured mode diameters of PSL particles with other sizes were within the ranges of the prescribed expanded uncertainty.

Text S3: Evaluation of HTDMA measurements using AS solution

To evaluate HTDMA performance for hygroscopic growth measurements, the hygroscopic growth of AS particles was measured using the HTDMA following the same procedure as that for WSM particles. Results were compared with those predicted using the E-AIM III model (Text S5, Fig. S2a). Here, the accuracy of RH measurements by Vaisala’s sensors is ≤ 2 % according to the manufacturer’s warranty. Smaller than expected deliquescence RH (DRH, between 70–75 % versus 80 % (Tang and Munkelwitz, 1994)) and efflorescence RH (ERH, approx. 30 % versus 37 % (Tang and Munkelwitz, 1994)) of AS might be the result of the history of RH in and downstream of NH₂, until AS particles were transferred to DMA2 in the HTDMA. The differences provide a guide to uncertainty of the DRH and ERH measurements.

Furthermore, for AS in the humidification branch, except at 85 % RH, and in the dehumidification branch at <65 % and 90 % RH, great disagreement was observed between measured and predicted κ_{AS} (predicted values deviated from those of measured ones by >15 %, Fig. S2b), which implies some bias of the measured RH and/or of analysis based on the E-AIM model. The considerable disagreement at low RH might be attributable to the assumption of perfectly spherical and non-porous solid AS particles, and might also be attributable to bias of the E-AIM model and uncertainty of the RH measurements. Because the differences would strongly affect quantitative analysis results if they rely on a combination of measurements and the E-AIM model, only data at 85 % in the humidification branch and the RH range of 65–85 % in the dehumidification branch were used to calculate the hygroscopicity parameters for WSOM (κ_{WSOM}) and EOM (κ_{EOM}).

Text S4: Sample blank evaluation and HTDMA measurement repeatability

Blank filters were extracted using the same procedure as that used for aerosol sample filters (Sect. 2.1).

Volume–size distributions of the obtained WSM particles were scanned using SMPS under dry conditions. Results (Fig. S3) show that the volume concentrations of the WSM particles obtained from the blank sample were much lower than those of the aerosol samples. At the dry diameter of 100 nm, the volume concentration of WSM particles from blank samples was, on average, 1.9 % (range 0.9 %–18 %) of those from aerosol samples. These results suggest that possible interference by non-volatile contaminants is, in general, small.

To assess the repeatability of the HTDMA analysis, the hygroscopic growth of WSM particles from sample OKNW_035 was measured three more times in both humidification and dehumidification modes more than five months after measurement of all extracted samples. Both extraction by water and measurement by HTDMA were repeated three times. Results of the additional three measurements are presented in Fig. S4. The standard deviations of g_f in the humidification (or dehumidification) branch were 0.01 (or 0.005), 0.02 (or 0.03), and 0.04 (or 0.02) respectively at 80, 85, and 90 %. The relative standard deviations of the measured g_f were smaller than 6 %, even in the RH range of 60–75 %, where deliquescence of the WSM aerosol particles might have occurred. The values of g_f from first measurements at 80, 85, and 90% RH were larger than the mean of the three repeat measurements in the humidification (or dehumidification) branch by 5.4 (or 3.2), 4.7 (or 5.6), and 3.0 (or 7.3) %, without correction for the slight difference of the sizing (Sect. 2.2) between DMA1 and DMA2. The first measurement was not included in the repeatability analysis because a possible change of the condition of the HTDMA during the long interval might have affected the result.

Text S5: Quantification of WSOM and WISOM based on mass spectra

The mass concentrations of WSOM and WISOM were determined using a phthalic acid method (Han et al., 2016) as follows. The mass spectra of WSOM (or WISOM), pure phthalic acid, and the mixtures of WSOM (or WISOM) and phthalic acid were obtained from offline AMS analysis. The mass ratios of WSOM (or WISOM) to phthalic acid in the mixtures (R_m) were calculated assuming the normalized mass spectra of the mixture are linear combinations of those of WSOM (or WISOM) and pure phthalic acid. For the calculation of R_m , the same relative ionization efficiency was applied for WSOM (or WISOM) and phthalic acid. The mass concentration of WSOM (or WISOM) (m_{OM} , $\mu\text{g m}^{-3}$) is calculable using Eq. S1 as shown below.

$$m_{OM} = \frac{10^6 R_m C_{ph} M_{ph} M_T A_T}{100 M_{ext} A_{ext} V_T} \quad (S1)$$

Therein, C_{ph} (weight %) represents the mass concentration of phthalic acid in water (or

dichloromethane/methanol) solution, M_{ph} (g) is the mass of the phthalic acid solution added to the mixture, M_{ext} (g) is the mass of the WSM (or WSOM) solution added to the mixture, M_T (g) is the total mass of the extracted WSM (or WSOM) solution, A_{ext} (cm²) is the area of the filter used for the extraction, A_T (cm²) is the total filter area subjected to aerosol sample collection, and V_T (m³) is the total volume of air sampled during the aerosol collection. The mass concentration of WSOM derived here shows good agreement with that derived as the product of WSOC from the TOC analyzer and the OM:OC of WSOM (Fig. S5). The consistent result supports the propriety of the quantification of WSOM and WSOC.

Text S6: Hygroscopic growth of WSM predicted using the E-AIM model

Hygroscopic growth of WSM without consideration of water uptake by WSOM and that of ammonium sulfate (AS) particles as a function of water activity (a_w) at 0.10 to 0.99, and also the corresponding hygroscopicity parameter (κ) were derived based on the output of the online E-AIM III model and the κ - Köhler theory as described below.

For application of the E-AIM III model to WSM, ammonium, sodium, and sulfate among quantified anions were considered because the concentrations of other ions were low (Table 3). Excess anions in each WSM solution were assumed to be in balance with protons electrically. The a_w range of 0.10–0.99 at a resolution of 0.01 was applied to each WSM solution and the AS solution at 298.15 K. In all calculations, the partitioning of HNO₃, HCl, H₂SO₄, and NH₃ to the gas phase was prevented. Furthermore, for the dehumidification branch, the formation of solids was also prevented. The quantity of water as a function of a_w in thermodynamically equilibrium conditions was obtained from the model. The hygroscopic growth factor was calculated as the ratio of the sum of the volumes of water and dry WSM (or AS) particle to the volume of dry WSM (or AS) particle. The volumes of dry WSIM and WSOM were calculated in the same manner as that stated in Text S7. The hygroscopicity parameter of WSM (κ_{WSM}), WSIM (κ_{inorg}), and AS (κ_{AS}) was derived following Eq. 2 in Petters and Kreidenweis (2007).

For WSM particles from atmospheric samples, the exponential part of the κ - Köhler equation, which represents the curvature (Kelvin) effect, was calculated on the assumption that the surface tension is that of pure water, the partial molar volume of water in the solution is equal to that of pure water, and that the volumes of WSOM in the particles were considered whereas the water uptake by the WSOM component was ignored. In the case of AS particles, the surface tension of the solution obtained from the E-AIM model was used instead for the calculation. The RH above the particle surface was then

calculated as the product of a_w and the corresponding exponential part. The κ_{WSM} and κ_{inorg} (or κ_{AS}) at the measured RH (i.e., 20, 30, 40, 50, 60, 65, 70, 75, 80, 85, and 90 %) were determined by looking up the a_w - κ_{WSM} - κ_{inorg} -RH (or a_w - κ_{AS} -RH) table at a resolution of 0.01.

Text S7: Derivation of volume concentrations of WSIM, WSOM, WISOM, and EC in PM_{0.95}

The chemical composition obtained from the offline analysis (Sect. 2.3) was used to derive the volume concentrations of WSIM, WSOM, WISOM, and EC for reconstruction of the hygroscopicity of WSOM, EOM and PM_{0.95}. To ascertain the volume concentration of WSIM, the respective contributions from potassium, calcium, magnesium, nitrate, and chloride were ignored because their contributions were minimal compared to those of sulfate, ammonium, and sodium (Table S3). Furthermore, sulfate in the dry condition was assumed to be present preferentially in the form of sodium sulfate (Na₂SO₄). The remaining sulfate was assumed to be present in the form of ammonium sulfate (AS, (NH₄)₂SO₄), letovicite (LET, (NH₄)₃H(SO₄)₂), ammonium hydrogen sulfate (AHS, NH₄HSO₄), and/or sulfuric acid (SA, H₂SO₄) according to the molar ratios of ammonium to the remaining sulfate ($R_{\text{A/S}}$) as follows: ammoniated sulfate was in the form of AS and LET for $1.5 < R_{\text{A/S}} \leq 2$, in the form of LET and AHS for $1 < R_{\text{A/S}} \leq 1.5$, and in the form of SA and AHS for $0 < R_{\text{A/S}} \leq 1$. The volume concentration of WSOM (or WISOM) was found as the ratio of its mass concentration to its density calculated using its O:C and H:C from the offline AMS analysis. The volume concentration of EOM was equal to the sum of the volume concentrations of WSOM and WISOM. The volume concentration of WSM was inferred as the sum of the volume concentrations of WSIM and WSOM. The volume concentration of EC was found using the EC mass concentration from OC/EC analysis, with the assumed density of 1.77 g cm⁻³ (Park et al., 2004).

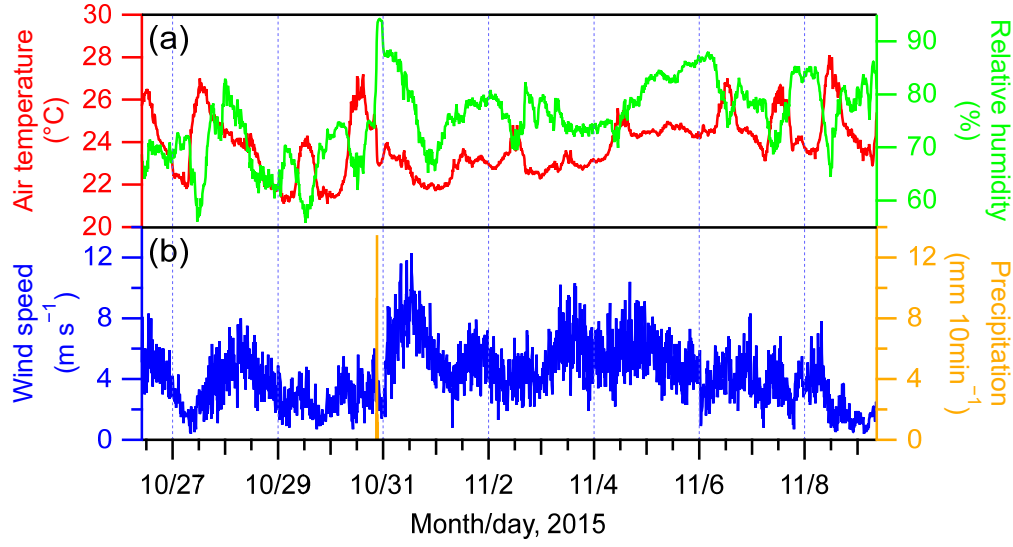


Figure S1: Time series of air temperature (°C), relative humidity (%), wind speed (m s⁻¹), and precipitation (mm 10-min⁻¹) during the sampling period for PM_{0.95}.

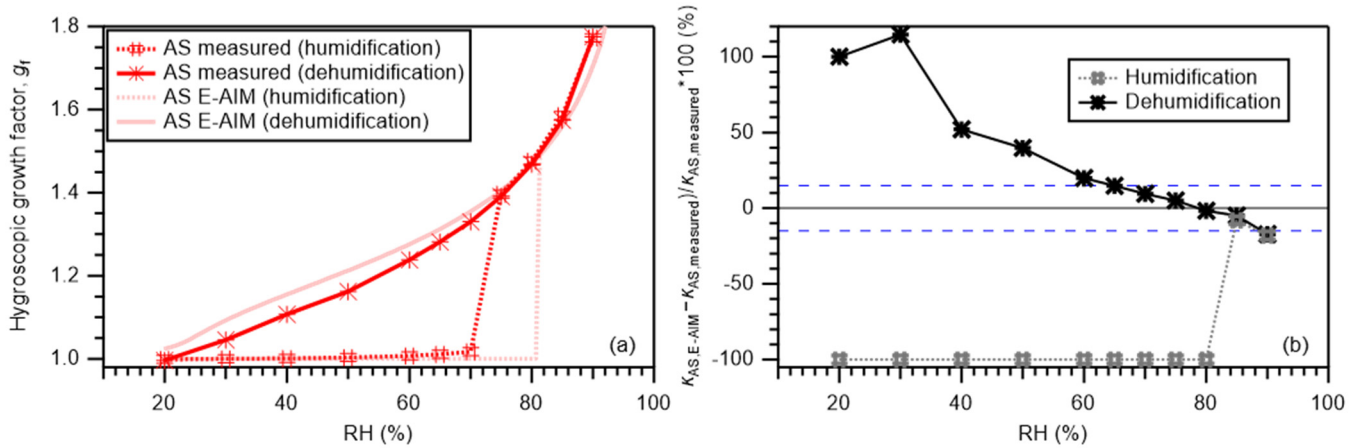


Figure S2: (a) Measured g_f and those predicted based on E-AIM in humidification and dehumidification branches for 100 nm ammonium sulfate (AS) particles. The predicted g_f in the dehumidification branch was obtained based on the assumption that solid salts are not formed. (b) Relative deviation of predicted κ_{AS} ($\kappa_{AS,E-AIM}$) from measured κ_{AS} ($\kappa_{AS,measured}$) in humidification and dehumidification branches. In both panels, markers represent individual data; lines are used to connect individual data points. The E-AIM predicted results in panel (a) are presented only by lines between points. Blue dashed lines in panel (b) represent +15 % and -15 %.

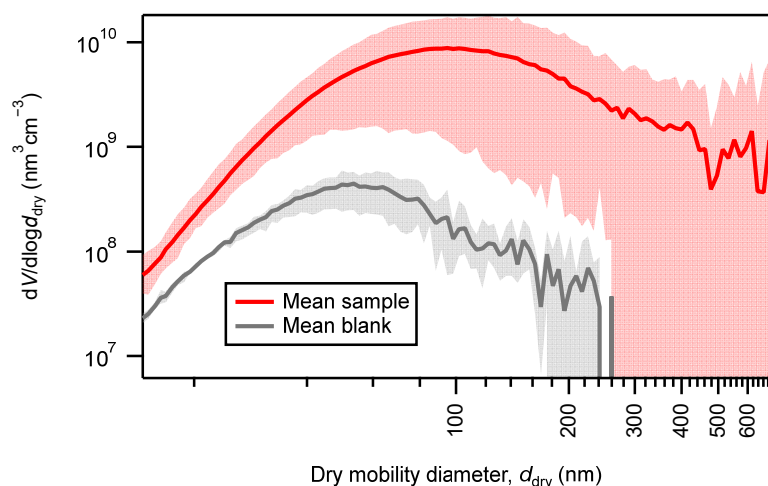


Figure S3: Volume–size distributions of WSM particles generated from ambient aerosol samples and blank samples. The red solid curve and shaded area respectively represent the means and ranges for all ambient aerosol samples. The gray solid curve and shaded area respectively represent the means and ranges of blank samples. Data below the range of the vertical axis are not shown.

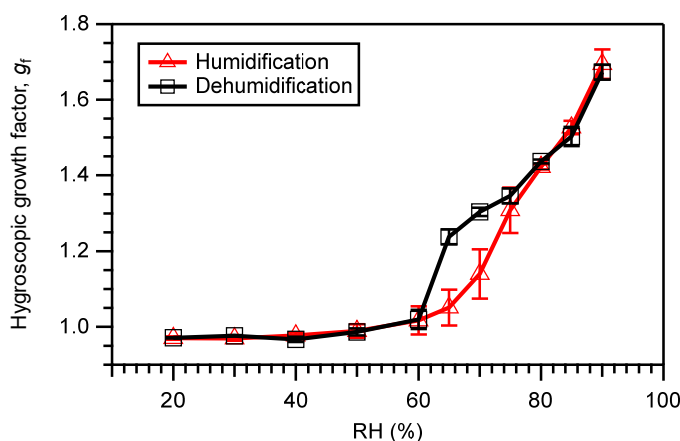


Figure S4: Results representing the repeatability of hygroscopic growth factor measurements: the g_f of 100 nm WSM particles from sample OKNW_035 as a function of RH. Markers and whiskers respectively represent mean values and standard deviations from three measurements (Text S4). The g_f values presented here are not corrected for the slight difference of the sizing (Sect. 2.2) between DMA1 and DMA2.

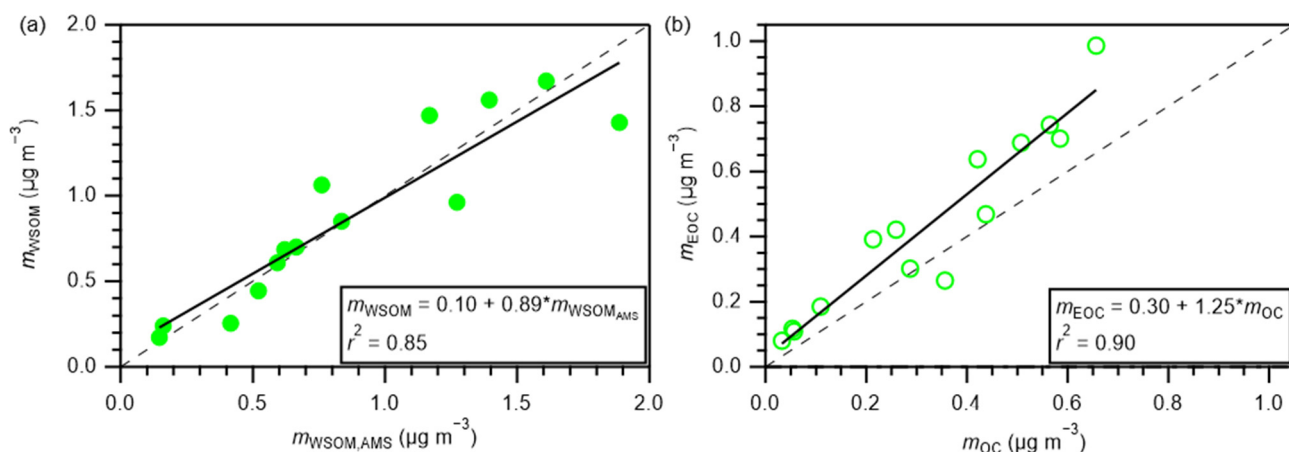


Figure S5: (a) Comparison of the mass concentrations of WSOM derived from WSOC from the TOC analyzer and the AMS-derived OM:OC of WSOM (m_{WSOM} ; Sect. 2.3), and those of WSOM from the AMS analysis using phthalic acid as the internal standard ($m_{\text{WSOM,AMS}}$; Text S5). (b) Comparison of the mass concentrations of EOC (m_{EOC}) from offline AMS analysis and those of OC (m_{OC}) from the thermal analysis. In both panels, solid and dashed lines respectively represent regression lines and 1:1 lines.

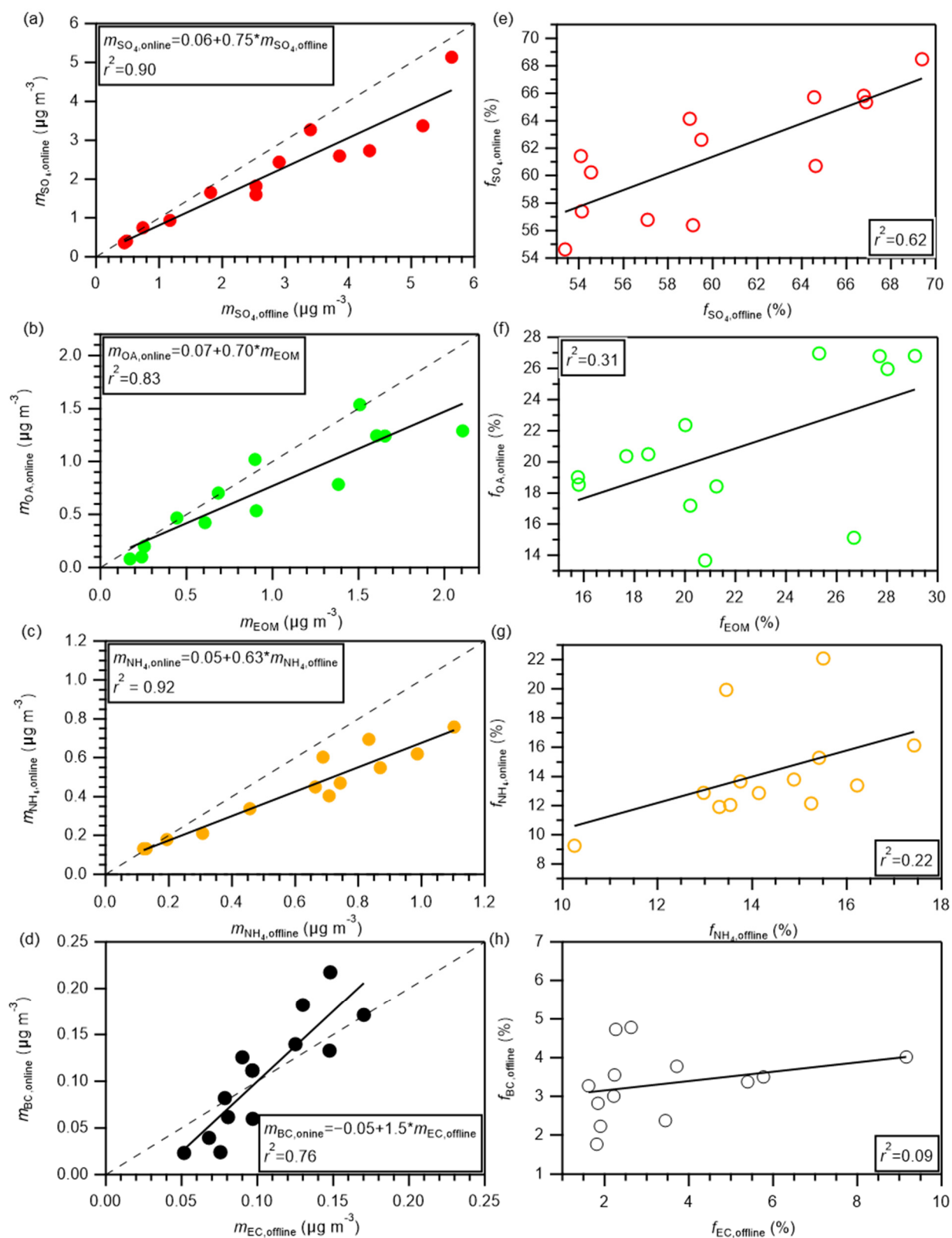


Figure S6: Comparison of the mass concentrations/fractions of chemical components in aerosols obtained from online and offline analyses: (a) mass concentrations of sulfate from online AMS analysis ($m_{\text{SO}_4, \text{online}}$) versus those from offline IC analysis ($m_{\text{SO}_4, \text{offline}}$); (b) mass concentrations of organics from

online AMS analysis ($m_{\text{OA,online}}$) and those from offline analysis (m_{EOM}); (c) mass concentrations of ammonium from online AMS analysis ($m_{\text{NH4,online}}$) versus those from offline IC analysis ($m_{\text{NH4,offline}}$); (d) mass concentrations of BC from online COSMOS analysis ($m_{\text{BC,online}}$) versus those from offline thermal analysis ($m_{\text{EC,offline}}$); (e) mass fractions of sulfate in the total mass of SO_4 , EOM, NH_4 , and BC from online analyses ($f_{\text{SO4,online}}$) versus those in the total mass of SO_4 , OA, NH_4 , and EC from the offline analyses ($f_{\text{SO4,offline}}$); (f) mass fractions of organics in the total mass of SO_4 , EOM, NH_4 , and BC from the online analyses ($f_{\text{OA,online}}$) versus those in the total mass of SO_4 , OA, NH_4 , and EC from offline analyses (f_{EOM}); (g) mass fractions of ammonium in the total mass of SO_4 , EOM, NH_4 , and BC from online analyses ($f_{\text{NH4,online}}$) versus those in the total mass of SO_4 , OA, NH_4 , and EC from offline analyses ($f_{\text{NH4,offline}}$); (h) mass fractions of BC in the total mass of SO_4 , EOM, NH_4 , and BC from online analyses ($f_{\text{BC,online}}$) versus those in the total mass of SO_4 , OA, NH_4 , and EC from offline analyses ($f_{\text{EC,offline}}$). Solid and dashed lines respectively show regression lines and 1:1 lines.

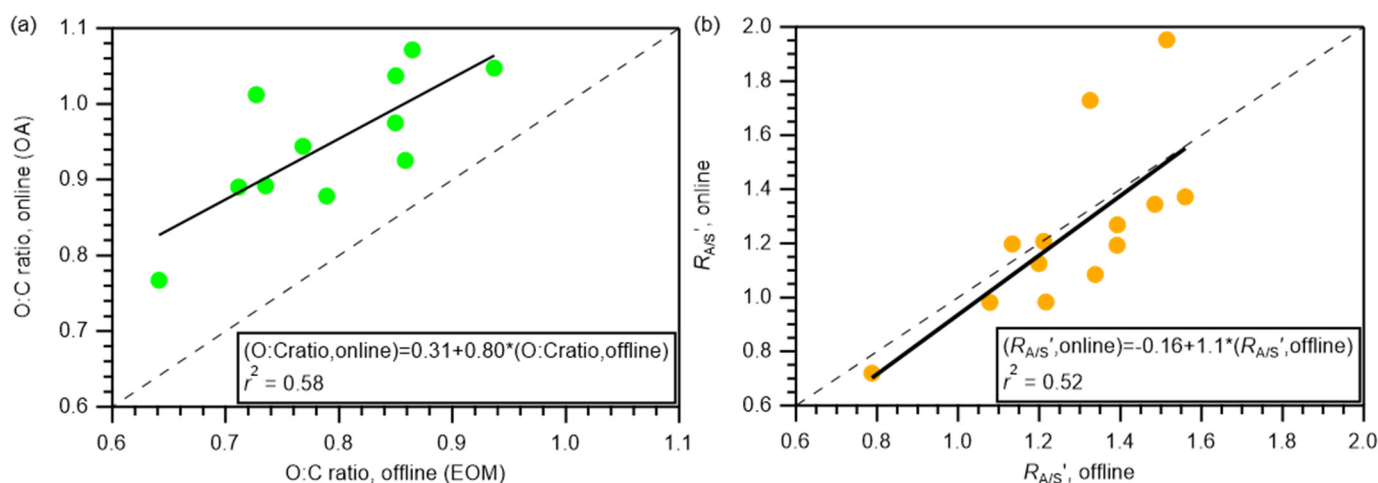


Figure S7: (a) Comparison of the O:C of OA from online analysis to those of EOM from offline analysis. (b) Comparison of the ammonium to sulfate ratio ($R_{\text{A/S'}}$) from online and offline analyses (Sect. 3.1). Solid and dashed lines respectively represent regression lines and 1:1 lines.

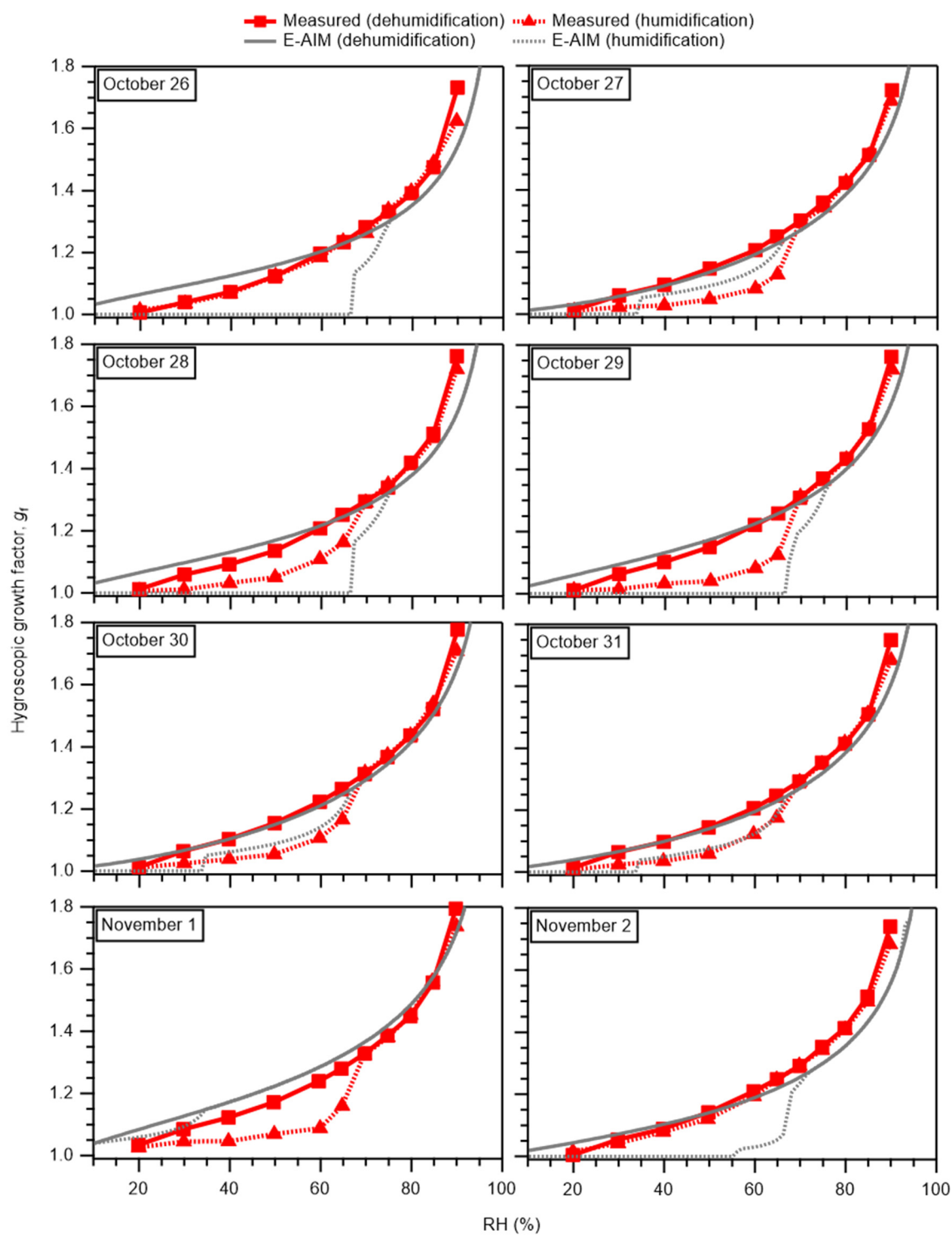


Figure S8: The g_f of 100 nm WSM particles in humidification and dehumidification branches as a function of RH for individual samples. The g_f predicted from the E-AIM model without considering the water retained by WSOM are also presented. Dates shown on panels represent dates when sampling started.

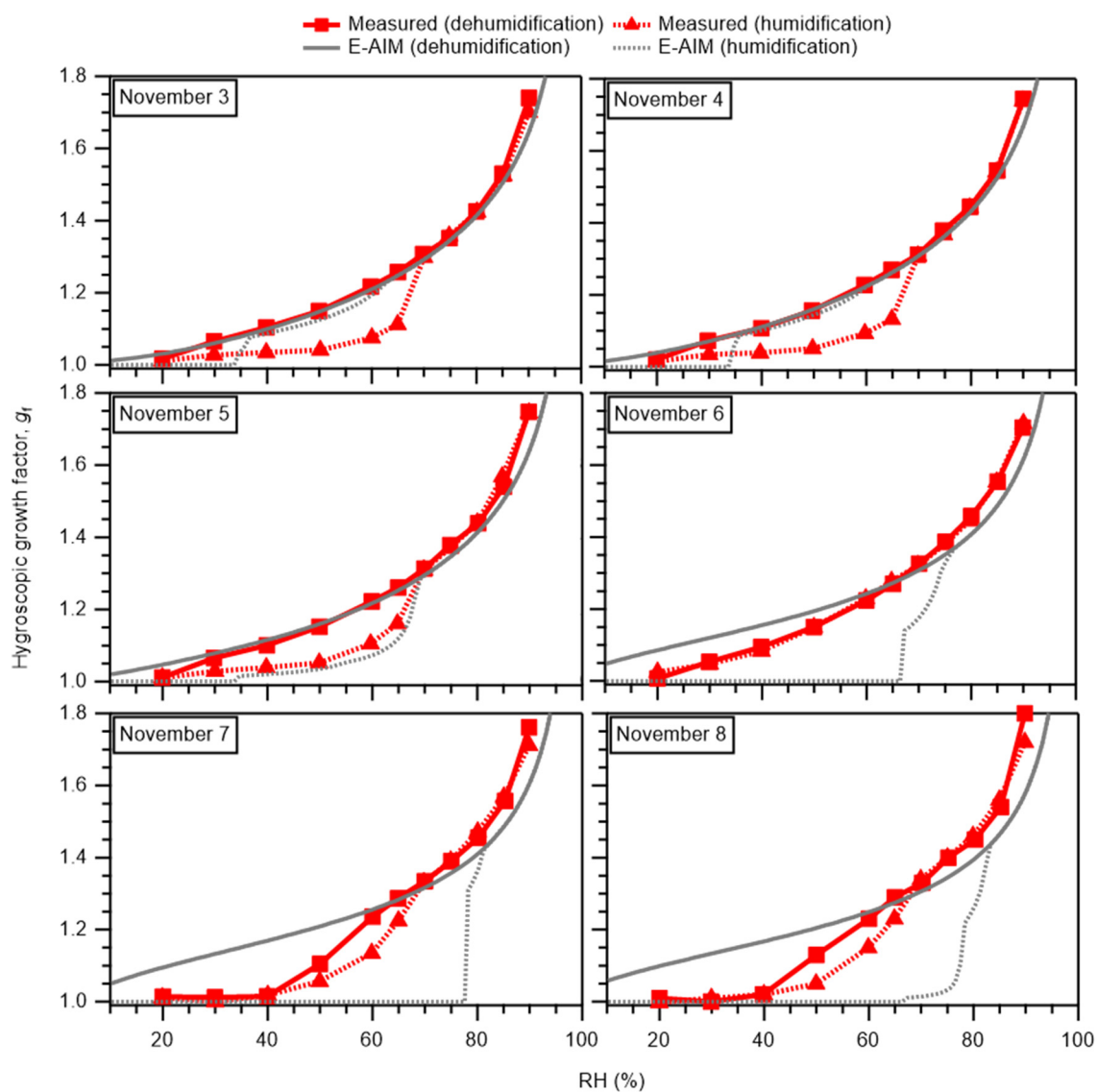


Figure S8 (continued)

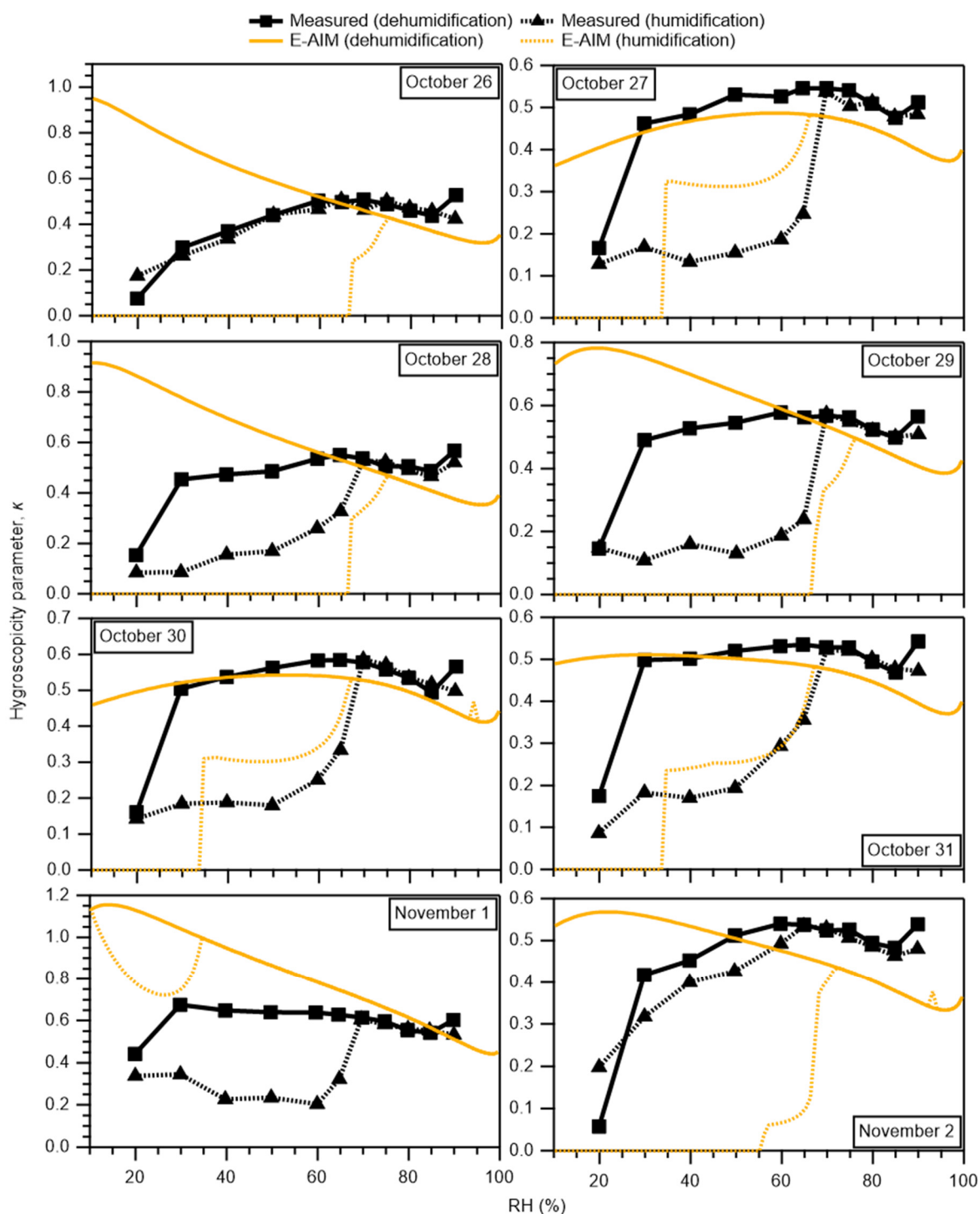


Figure S9: The κ_{WSM} of 100 nm WSM particles in humidification and dehumidification branches as a function of RH. The κ_{WSM} values predicted from the E-AIM model without consideration of water retained by WSOM are also shown. Dates shown on panels represent dates when sampling started.

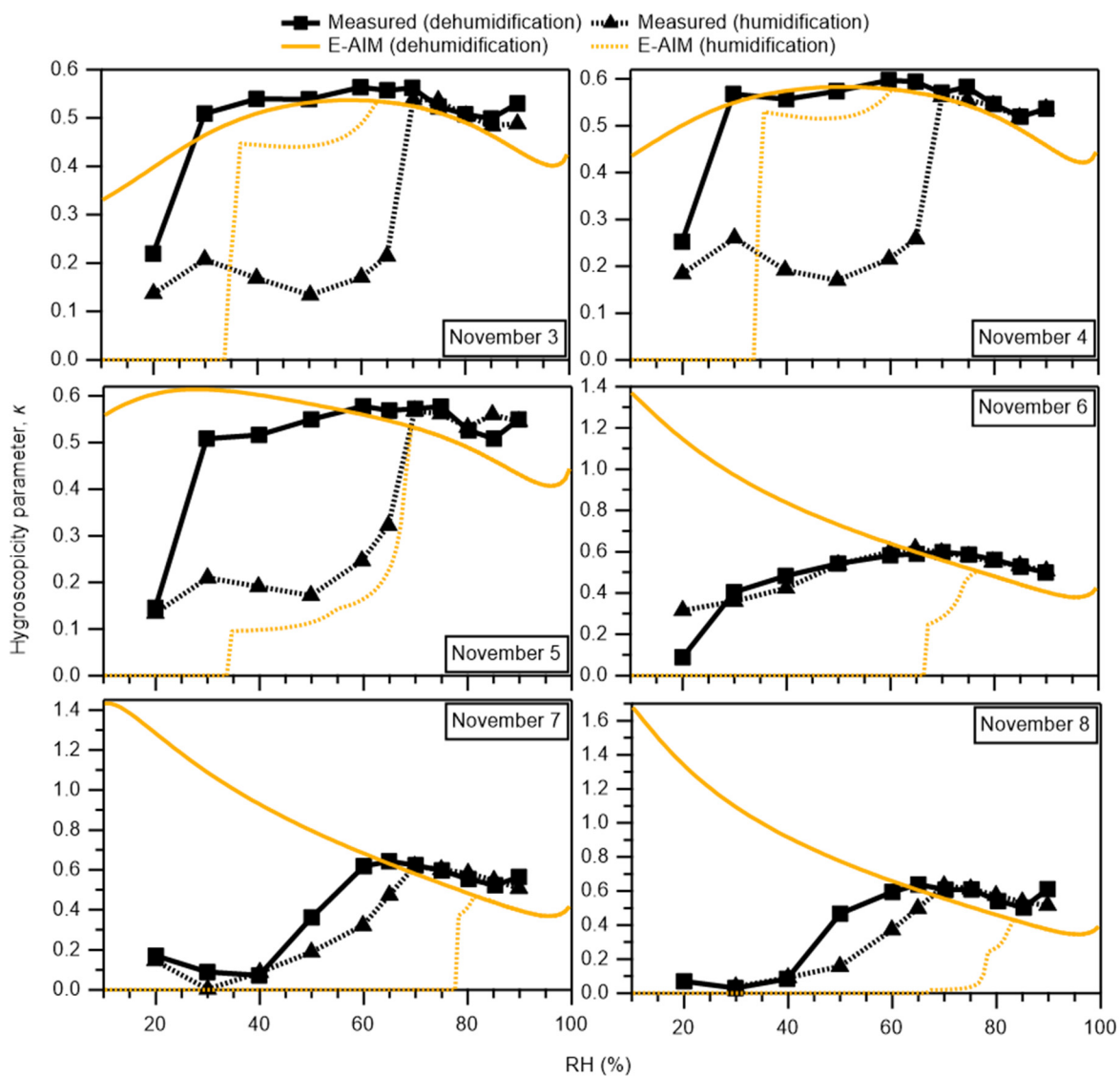


Figure S9 (continued)

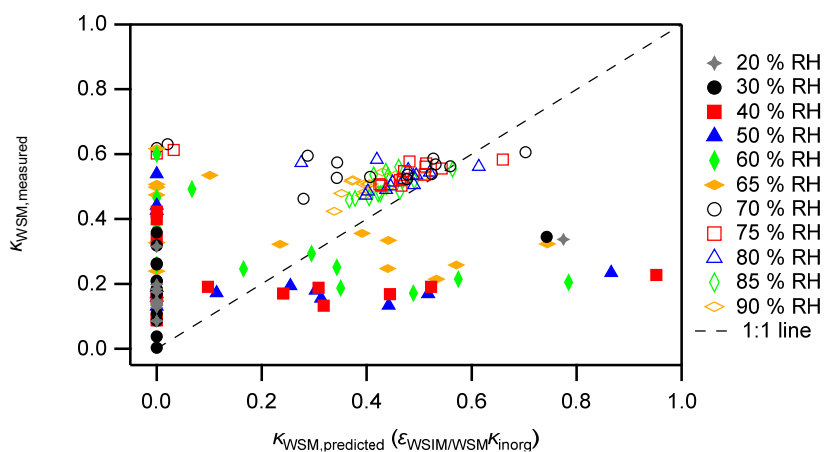


Figure S10: Measured versus predicted κ_{WSM} at different RH. The dashed line is the 1:1 line.

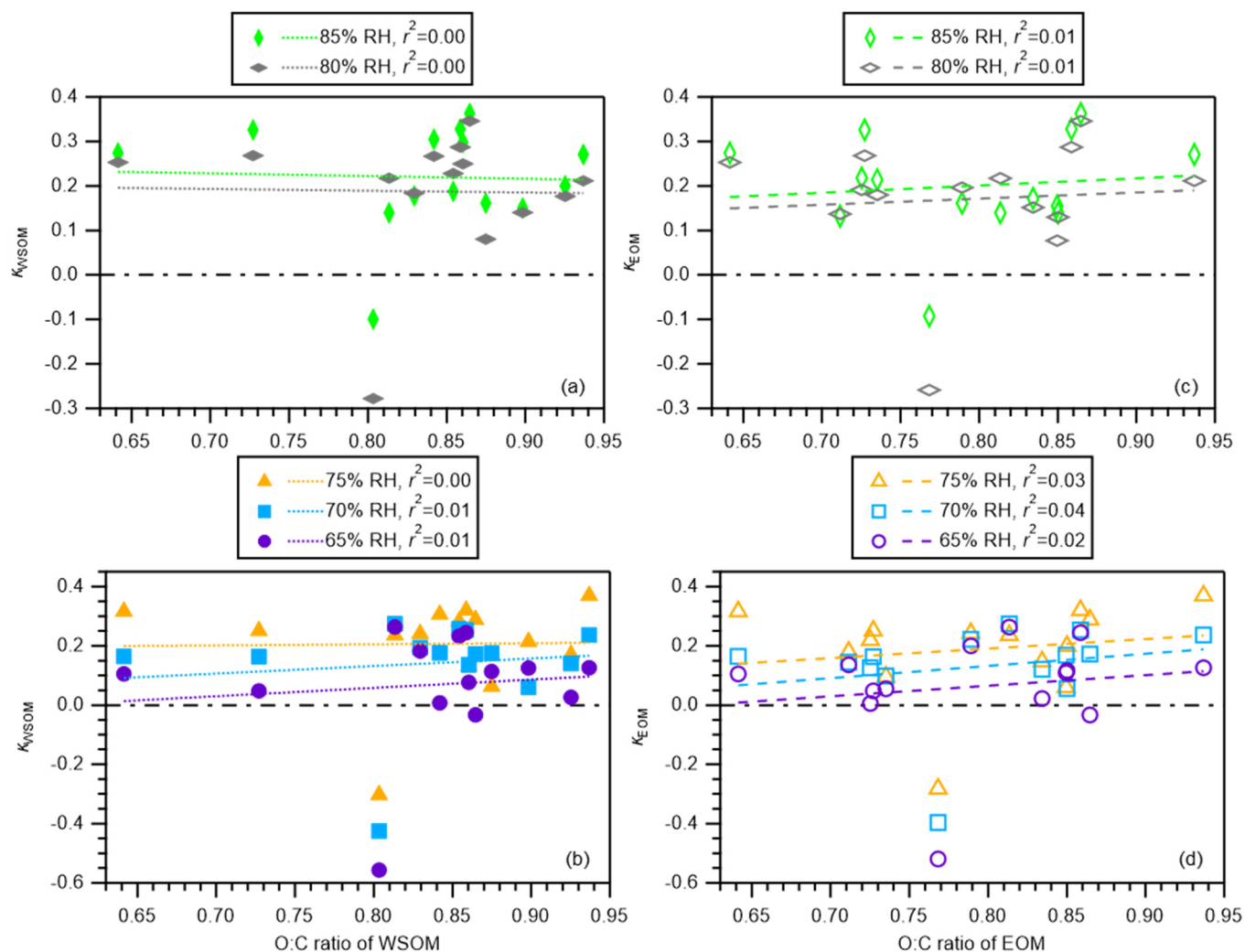


Figure S11: (a and b) Scatter plots of κ_{WSOM} versus O:C of WSOM at (a) 80 and 85 % RH and at (b) 65, 70, and 75 % RH. (c and d) Scatter plots of κ_{EOM} versus O:C of EOM at (c) 80 and 85 % RH and at (d) 65, 70, and 75 % RH.

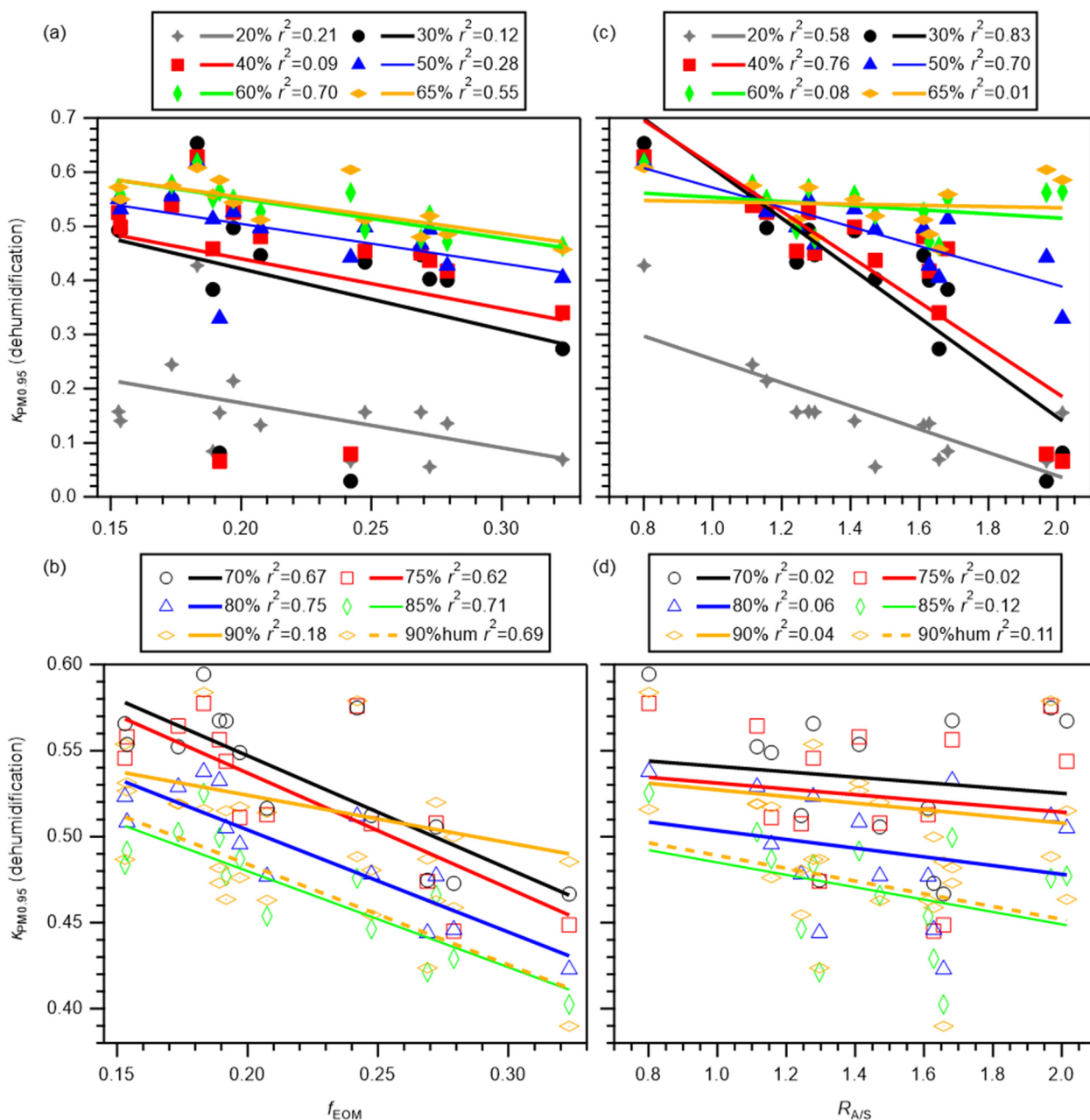


Figure S12: The $\kappa_{PM0.95}$ values in the dehumidification branch versus (a and b) mass fractions of EOM in PM0.95 (f_{EOM}) and (c and d) the ammonium-to-remaining sulfate molar ratio ($R_{A/S}$) from offline analysis. Panels a and c present results obtained for 20, 30, 40, 50, 60, and 65 % RH. Panels c and d present results obtained for 70, 75, 80, 85, and 90% RH. The $\kappa_{PM0.95}$ at 90 % RH in the humidification branch (90%hum) was also compared to (b) f_{WSOM} and (d) $R_{A/S}$. Coefficients of determination r^2 are also presented.

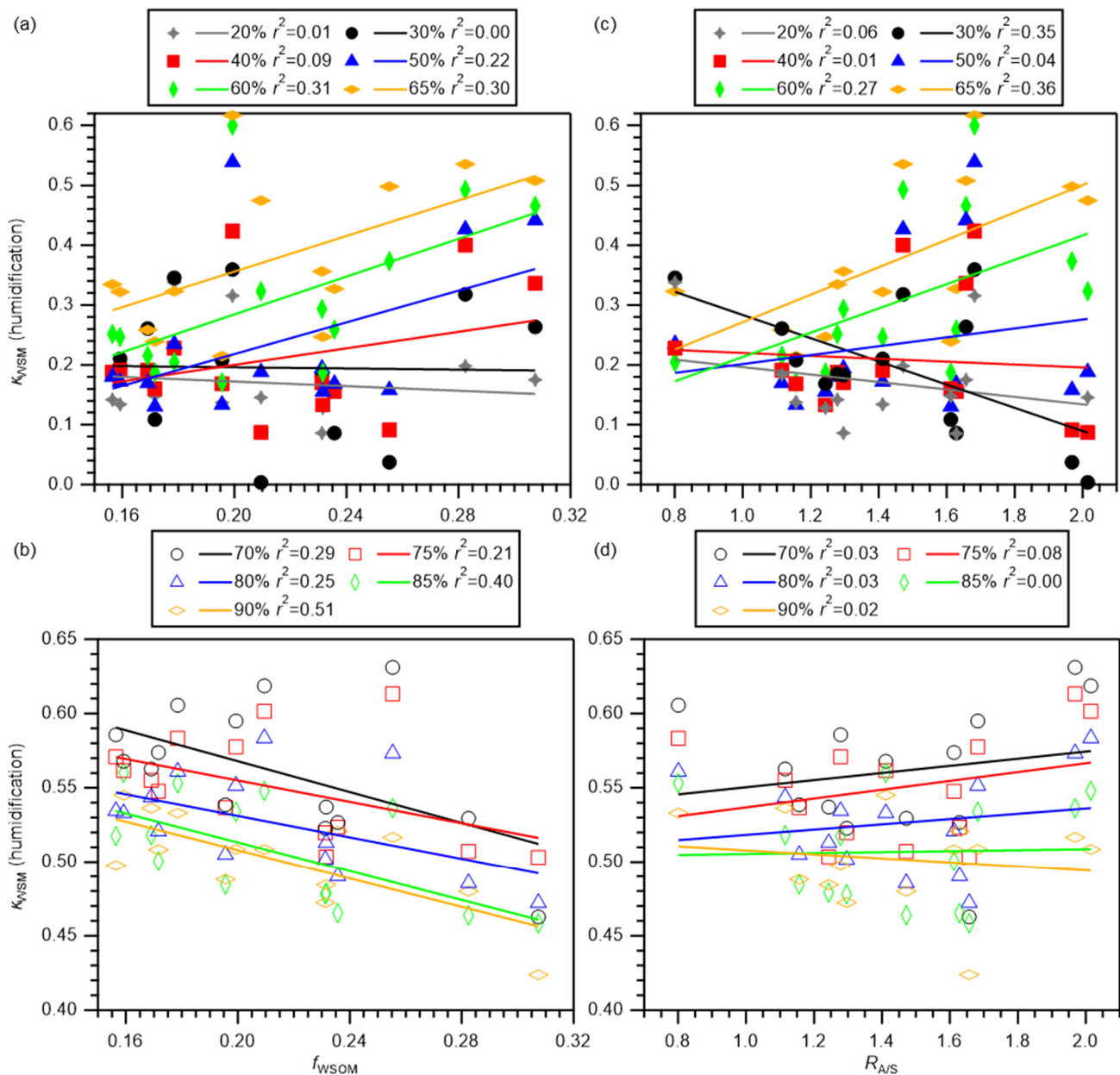


Figure S13: The κ_{WSM} values in the humidification branch versus (a and b) mass fractions of WSOM in WSM (f_{WSOM}) and (c and d) the ammonium-to-remaining sulfate molar ratio ($R_{\text{A/S}}$) from offline analysis. Panels a and c present results obtained for 20, 30, 40, 50, 60, and 65 % RH. Panels c and d present results obtained for 70, 75, 80, 85, and 90 % RH. Coefficients of determination r^2 are also shown.

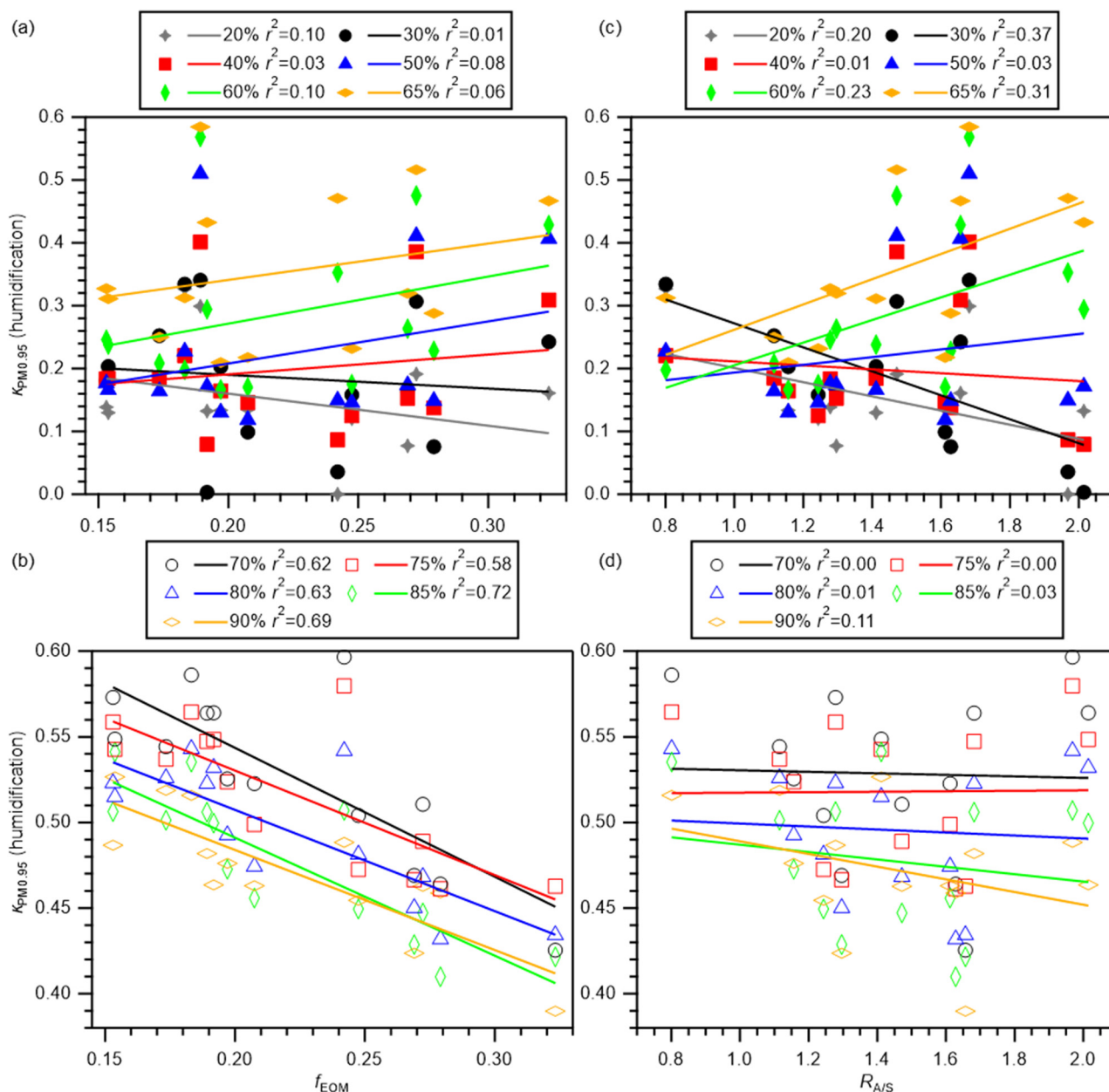


Figure S14: The $\kappa_{PM0.95}$ values in the humidification branch versus (a and b) the mass fractions of EOM in $PM_{0.95}$ (f_{EOM}) and (c and d) the ammonium-to-remaining sulfate molar ratio ($R_{A/S}$) from offline analysis. Panels a and c present results obtained for 20, 30, 40, 50, 60, and 65 % RH. Panels c and d present results obtained for 70, 75, 80, 85, and 90 % RH. Coefficients of determination r^2 are also presented.

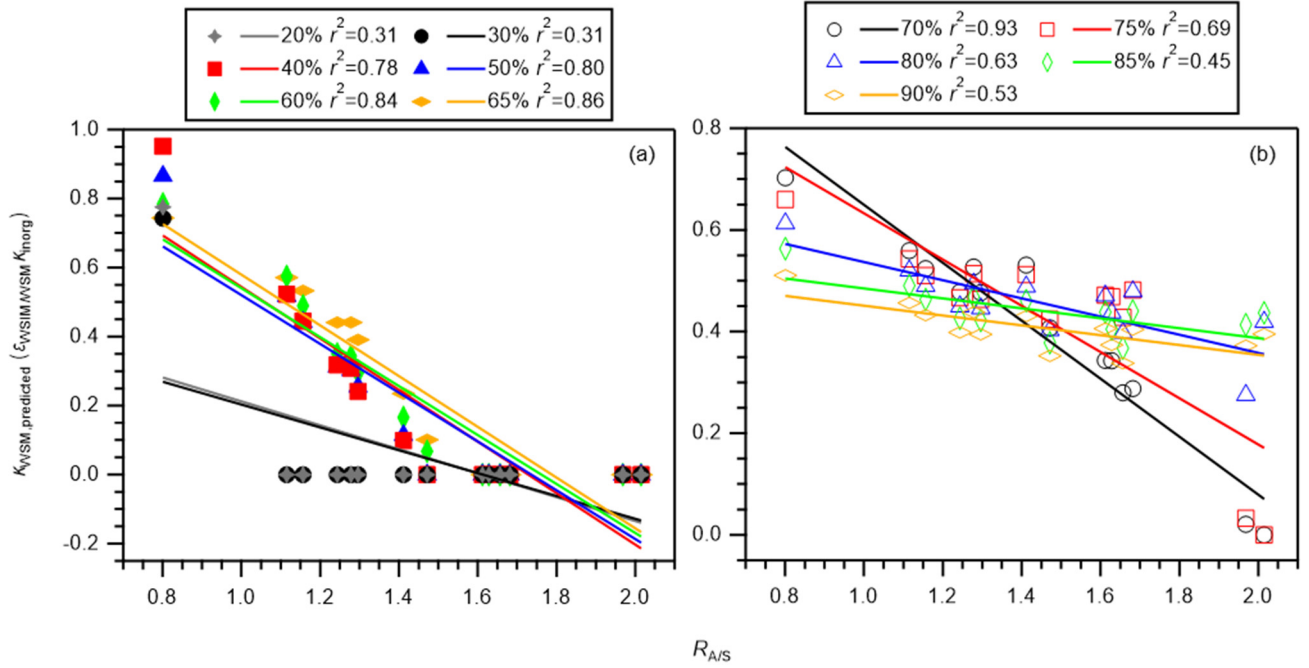


Figure S15: Scatter plots of predicted κ_{WSM} versus $R_{A/S}$ of WSM at (a) 20, 30, 40, 50, 60, and 65 % RH and (b) 70, 75, 80, 80, and 90 % RH. Markers and lines respectively represent individual data and regression lines. Coefficients of determination are also presented.

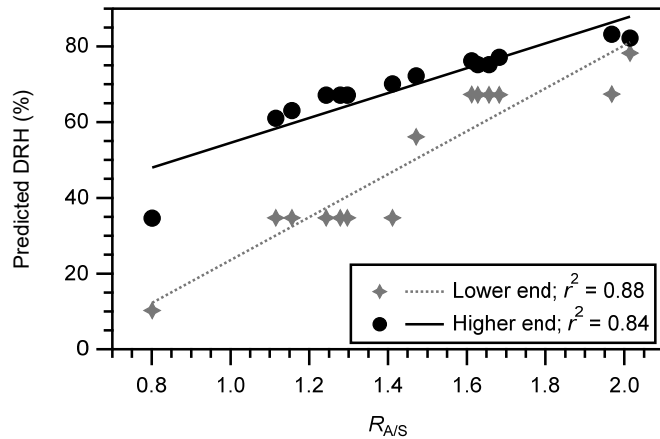


Figure S16: Scatter plots of DRH predicted by E-AIM versus $R_{A/S}$ of WSM. Gray stars present the predicted RH at which the g_f in the humidification branch became greater than unity, and the solid line represents the corresponding regression line. Black circles show the predicted RH at which the g_f in the humidification and dehumidification branches became identical, and the dotted line represents the corresponding regression line.

Table S1: Sampling periods and sampled air volumes for the PM_{0.95} studied

Sample ID	Period (in 2015, JST)	Air volume (m³)
OKNW_001	26 Oct, 09:56:00 – 27 Oct, 09:00:03	1569.5
OKNW_003	27 Oct, 09:26:00 – 28 Oct, 09:00:00	1602.9
OKNW_005B*	28 Oct, 09:11:11 – 28 Oct, 09:11:21	0
OKNW_006	28 Oct, 09:43:30 – 29 Oct, 09:00:00	1584.5
OKNW_009	29 Oct, 09:24:00 – 30 Oct, 09:00:00	1608.7
OKNW_011	30 Oct, 09:23:00 – 31 Oct, 09:00:00	1612.5
OKNW_014	31 Oct, 09:46:00 – 1 Nov, 09:00:00	1588.1
OKNW_017	1 Nov, 09:34:10 – 2 Nov, 09:00:01	1602.8
OKNW_019B*	2 Nov, 09:39:00 – 2 Nov, 09:39:10	0
OKNW_020	2 Nov, 09:59:45 – 3 Nov, 09:00:00	1574.7
OKNW_023	3 Nov, 09:20:00 – 4 Nov, 09:00:00	1621.2
OKNW_025	4 Nov, 09:22:40 – 5 Nov, 09:00:00	1619.9
OKNW_028	5 Nov, 09:44:40 – 6 Nov, 09:00:00	1595.9
OKNW_045B*	6 Nov, 09:19:20 – 6 Nov, 09:19:30	0
OKNW_032	6 Nov, 09:49:30 – 7 Nov, 09:00:00	1590.7
OKNW_035	7 Nov, 09:24:40 – 8 Nov, 09:00:02	1619.8
OKNW_037	8 Nov, 09:25:00 – 9 Nov, 09:00:00	1620.2
OKNW_039B*	9 Nov, 09:16:00 – 9 Nov, 09:16:10	0

* Field blanks

Table S2: Mode diameters of PSL size standards measured using DMA1, DMA2, and SMPS (in nm)^a

Manufacturer's warranty^b	HTDMA		Online SMPS
	DMA1	DMA2	
55 (± 1)	-	61.8 ± 0.3	60.3 ± 0.2
100 (± 3)	100.8 ± 0.0	103.2 ± 0.2	102.8 ± 0.3
309 (± 9)	303.3 ± 0.2	314.8 ± 1.1	307.5 ± 0.2 (308.4 ± 0.3)
498 (± 9)	-	516.7 ± 1.2	503.4 ± 0.5

^a The mean ± SD of the mode diameters from fittings. Results are based on calibrations done before analysis of atmospheric samples, except for the case of 309 nm PSL size standards from the SMPS, for which calibration was also made after sample analysis (in parenthesis).

^b Mean diameter (± expanded uncertainty; $k = 2$).

Table S3: Mass concentrations of water-soluble ions ($\mu\text{g m}^{-3}$) and water-soluble organic carbon (WSOC, $\mu\text{gC m}^{-3}$) in $\text{PM}_{0.95}$ ^a

Sample ID	MSA	Cl^-	NO_3^-	SO_4^{2-}	NH_4^+	Na^+	K^+	Ca^{2+}	Mg^{2+}	WSOC
OKNW_001	0.0107	BDL	0.0033	1.5761	0.4333	0.0877	0.045	0.0079	0.0118	0.4022
OKNW_003	0.0316	BDL	0.0035	3.8618	0.8696	0.0656	0.0594	0.0105	0.0099	0.6412
OKNW_006	0.025	0.0017	0.0063	2.5378	0.7076	0.1069	0.0519	0.0224	0.0147	0.4613
OKNW_009	0.0157	BDL	0.0025	2.5371	0.743	0.0396	0.0418	0.0126	0.0053	0.3079
OKNW_011	0.0154	BDL	0.0015	2.9046	0.6634	0.0677	0.0415	0.0087	0.0089	0.3015
OKNW_014	0.0413	0.0012	0.0091	4.3392	0.9866	0.1371	0.0482	0.0124	0.0194	0.7385
OKNW_017	0.0425	BDL	0.0052	5.6403	0.8334	0.0475	0.0327	0.0068	0.0091	0.6412
OKNW_020	0.0098	0.0016	0.0043	1.1744	0.3069	0.0306	0.0152	0.0063	0.0049	0.2646
OKNW_023	0.0399	0.0006	0.0054	5.1817	1.1029	0.0483	0.0592	0.0063	0.0068	0.673
OKNW_025	0.0249	BDL	0.0019	3.3991	0.6882	0.0536	0.0301	0.0057	0.0077	0.3632
OKNW_028	0.0209	BDL	0.0017	1.8159	0.4562	0.0453	0.0165	0.0059	0.0055	0.1845
OKNW_032	0.0109	BDL	0.0008	0.7429	0.1942	0.0613	0.0108	0.0053	0.0074	0.1091
OKNW_035	0.0054	BDL	0.0006	0.4499	0.1279	0.0535	0.0056	0.0044	0.0054	0.0796
OKNW_037	0.0074	0.0006	0.0018	0.4839	0.1204	0.0757	0.0042	0.0047	0.0051	0.1169
Mean	0.0215	0.0059	0.0034	2.6175	0.5881	0.0657	0.0330	0.0086	0.0087	0.3775

^a Data were corrected for field blanks. BDL, below detection limit (i.e., mean + three times standard deviation of blank samples).

Table S4: Mean \pm standard deviation of g_f , κ_{WSM} , $\kappa_{PM0.95}$, κ_{WSOM} , and κ_{EOM} in humidification and dehumidification branches

RH (%)	Humidification					Dehumidification				
	g_f	κ_{WSM}	$\kappa_{PM0.95}$	κ_{WSOM}	κ_{EOM}	g_f	κ_{WSM}	$\kappa_{PM0.95}$	κ_{WSOM}	κ_{EOM}
20	1.01 \pm 0.01	0.17 \pm 0.08	0.15 \pm 0.08	-	-	1.01 \pm 0.01	0.17 \pm 0.10	0.16 \pm 0.09	-	-
30	1.03 \pm 0.01	0.20 \pm 0.11	0.19 \pm 0.11	-	-	1.05 \pm 0.02	0.42 \pm 0.18	0.40 \pm 0.17	-	-
40	1.04 \pm 0.02	0.21 \pm 0.10	0.20 \pm 0.10	-	-	1.09 \pm 0.03	0.45 \pm 0.17	0.42 \pm 0.16	-	-
50	1.07 \pm 0.04	0.24 \pm 0.13	0.22 \pm 0.12	-	-	1.14 \pm 0.02	0.52 \pm 0.07	0.49 \pm 0.07	-	-
60	1.13 \pm 0.05	0.30 \pm 0.13	0.29 \pm 0.12	-	-	1.22 \pm 0.01	0.57 \pm 0.04	0.54 \pm 0.05	-	-
65	1.18 \pm 0.05	0.38 \pm 0.13	0.35 \pm 0.12	-	-	1.26 \pm 0.02	0.57 \pm 0.04	0.54 \pm 0.05	0.07 \pm 0.20	0.06 \pm 0.19
70	1.31 \pm 0.02	0.56 \pm 0.05	0.53 \pm 0.05	-	-	1.31 \pm 0.02	0.57 \pm 0.04	0.53 \pm 0.04	0.14 \pm 0.17	0.13 \pm 0.16
75	1.36 \pm 0.02	0.55 \pm 0.04	0.52 \pm 0.04	-	-	1.37 \pm 0.02	0.56 \pm 0.04	0.52 \pm 0.04	0.21 \pm 0.17	0.19 \pm 0.16
80	1.43 \pm 0.02	0.53 \pm 0.03	0.50 \pm 0.04	-	-	1.43 \pm 0.02	0.52 \pm 0.03	0.49 \pm 0.04	0.19 \pm 0.15	0.17 \pm 0.14
85	1.53 \pm 0.03	0.51 \pm 0.04	0.48 \pm 0.04	0.26 \pm 0.15	0.24 \pm 0.15	1.53 \pm 0.02	0.50 \pm 0.03	0.47 \pm 0.03	0.22 \pm 0.12	0.20 \pm 0.11
90	1.71 \pm 0.03	0.50 \pm 0.03	0.47 \pm 0.04	-	-	1.75 \pm 0.03	0.55 \pm 0.03	0.52 \pm 0.03	-	-

Table S5: Fractional contribution of WSOM to the κ values of WSM and PM_{0.95} (mean \pm standard deviation, %)

RH (%)	Humidification		Dehumidification	
	$(\varepsilon_{WSOM/WSM} \times \kappa_{WSOM}) / \kappa_{WSM} \times 100$	$(\varepsilon_{WSOM/PM0.95} \times \kappa_{WSOM}) / \kappa_{PM0.95} \times 100$	$(\varepsilon_{WSOM/WSM} \times \kappa_{WSOM}) / \kappa_{WSM} \times 100$	$(\varepsilon_{WSOM/PM0.95} \times \kappa_{WSOM}) / \kappa_{PM0.95} \times 100$
65	-	-	4 \pm 8	4 \pm 8
70	-	-	7 \pm 7	7 \pm 7
75	-	-	10 \pm 7	10 \pm 7
80	-	-	10 \pm 7	10 \pm 7
85	13 \pm 7	13 \pm 7	12 \pm 7	12 \pm 7

References

- Chen, Q., Ikemori, F., Nakamura, Y., Vodicka, P., Kawamura, K., and Mochida, M.: Structural and light-absorption characteristics of complex water-insoluble organic mixtures in urban submicrometer aerosols, *Environmental Science & Technology*, 51, 8293-8303, 10.1021/acs.est.7b01630, 2017.
- Han, Y. M., Kawamura, K., Chen, Q. C., and Mochida, M.: Formation of high-molecular-weight compounds via the heterogeneous reactions of gaseous C-8-C-10 n-aldehydes in the presence of atmospheric aerosol components, *Atmospheric Environment*, 126, 290-297, 10.1016/j.atmosenv.2015.11.050, 2016.
- Park, K., Kittelson, D. B., Zachariah, M. R., and McMurry, P. H.: Measurement of inherent material density of nanoparticle agglomerates, *J. Nanopart. Res.*, 6, 267-272, 10.1023/B:NANO.0000034657.71309.e6, 2004.
- Petters, M. D., and Kreidenweis, S. M.: A single parameter representation of hygroscopic growth and cloud condensation nucleus activity, *Atmospheric Chemistry and Physics*, 7, 1961-1971, 10.5194/acp-7-1961-2007, 2007.
- Tang, I. N., and Munkelwitz, H. R.: Water Activities, Densities, and Refractive-Indexes of Aqueous Sulfates and Sodium-Nitrate Droplets of Atmospheric Importance, *Journal of Geophysical Research-Atmospheres*, 99, 18801-18808, 10.1029/94jd01345, 1994.